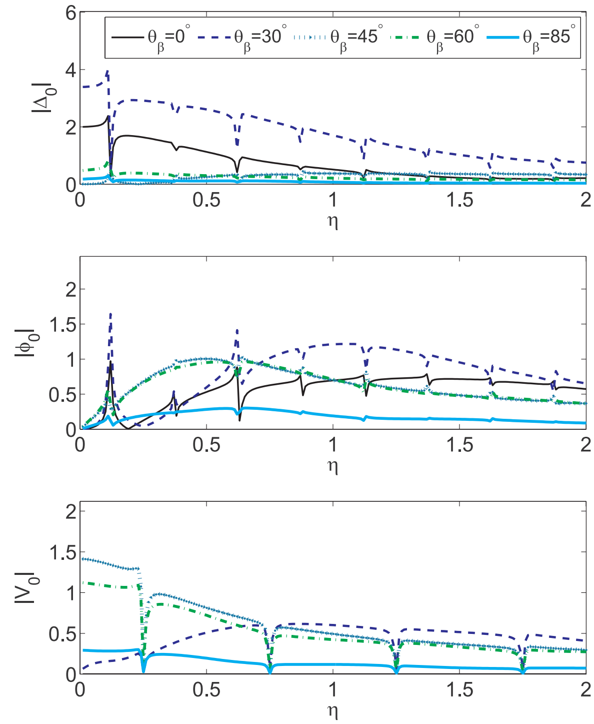

Fig. 6. Spectra of foundation displacements from "relaxed" solutions. $a/h = 1$, $W/H = 1$, $H/a = 2$, $m_b/m_f = 2$, and $\varepsilon = 4$.

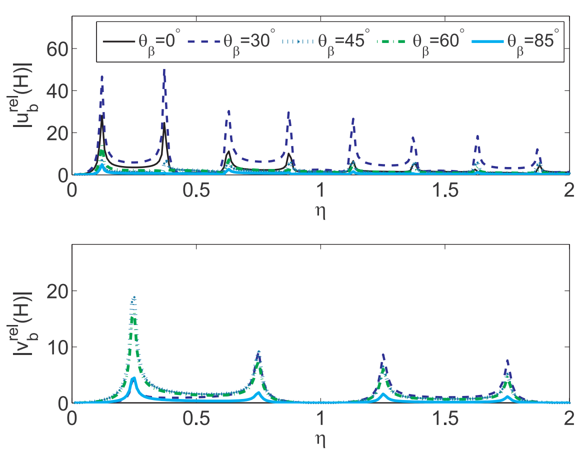

Fig. 7. Spectra of relative displacements of the shear wall from "relaxed" solutions. $a/h = 1$, $W/H = 1$, $H/a = 2$, $m_b/m_f = 2$, and $\varepsilon = 4$.

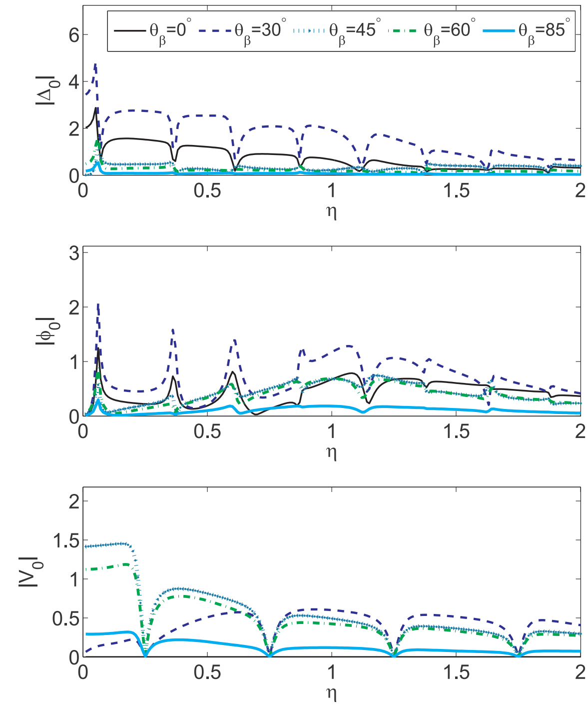

Fig. 8. Spectra of foundation displacements from "relaxed" solutions. $a/h = 1$, $W/H = 0.25$, $H/a = 8$, $m_b/m_f = 8$, and $\varepsilon = 4$.

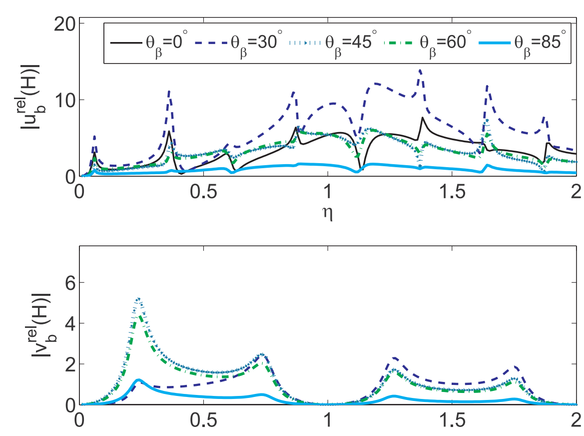

Fig. 9. Spectra of relative displacements of the shear wall from "relaxed" solutions. $a/h = 1$, $W/H = 0.25$, $H/a = 8$, $m_b/m_f = 8$, and $\varepsilon = 4$.

profiles that separate the case of $\theta_\beta < \theta_{cr}$ and $\theta_\beta > \theta_{cr}$ are exhibited, particularly in Figs. 2 and 6. For $\theta_\beta = 0°$ and $\theta_\beta = 30°$, in addition to the large response with high peak values near the first few natural frequencies (due to the coupling with the large horizontal translation of the foundation $|\Delta_0|$ at these two incident angles), $|\phi_0|$ do not grow as fast as in the cases of $\theta_\beta = 45°$ and $\theta_\beta = 60°$. In between the natural frequencies, the foundation rotations are significant when $\theta_\beta = 45°$ and $\theta_\beta = 60°$, with the local maxima at around $\eta \approx 0.5$ in Figs. 2 and 6. At $\theta_\beta = 85°$, despite the smaller values at all frequencies, $|\phi_0|$ also has similar behavior as $\theta_\beta = 45°$ and $\theta_\beta = 60°$. The differences between these two types of behavior become less apparent for a taller shear wall as shown in Figs. 4 and 8, in which it can be seen that the local maxima of $|\phi_0|$ for $\theta_\beta = 45°$ and $\theta_\beta = 60°$ occur near $\eta \approx 1.1$.

In the range where η is smaller than the first horizontal/vertical resonant frequencies, $|\Delta_0|$ and $|u_b^{rel}(H)|$ are larger when the incident angle makes $|u_x^{ff}(z=0)|$ larger; similarly, $|V_0|$ and $|v_b^{rel}(H)|$ are larger when the incident angle makes $|u_z^{ff}(z=0)|$ larger. This order starts to change beyond the first resonant frequency due to the interplay between the foundation filtering effect and the interactions previously described. The order change is especially prominent for $|V_0|$ when η is approaching 2 in Figs. 2, 4, 6 and 8.

Comparing the spectra of a taller shear wall with those of the square wall (comparing Figs. 8 and 9 with Figs. 6 and 7, or Figs. 4 and 5 with Figs. 2 and 3), it can be seen that for the taller shear wall, the first peaks of $|\Delta_0|$ and $|\phi_0|$ shift more toward lower frequencies with the slightly higher peak value for $|\Delta_0|$. The most dramatic changes for the taller shear wall are in the spectra of $|u_b^{rel}(H)|$: the first few peak values are considerably reduced from the corresponding square shear wall, with the first peak being more than 5 times smaller. In between natural frequencies in the range from $\eta \approx 0.8$ to $\eta \approx 1.4$, the value of $|u_b^{rel}(H)|$ can be larger than the first few peak values in the same spectrum. This region also corresponds to a relatively larger $|\phi_0|$ compared with other frequencies away from resonance.

Comparing the results with a shallow foundation to those of a semi-circular foundation (comparing Figs. 2 and 3 with Figs. 6 and 7 for the square shear wall, or Figs. 4 and 5 with Figs. 8 and 9 for the tall shear wall), it can be seen that for a shallower foundation depth with $\theta_\beta = 0°$ and $\theta_\beta = 30°$, $|\Delta_0|$ decreases in a slower rate as η increases for the whole frequency range $0 < \eta \leq 2$. However, $|u_b^{rel}(H)|$ and $|v_b^{rel}(H)|$ are smaller at lower frequencies with the smaller peak values, and the first peak of $|v_b^{rel}(H)|$ at $\theta_\beta = 30°$ even disappears as can be seen in Figs. 3 and 7. As for rotation, the change of $|\phi_0|$ highly depends on the incident angle: at $\theta_\beta = 45°$ and $\theta_\beta = 60°$, $|\phi_0|$ grows to a larger local maxima (the approximate location of the local maxima are unchanged: at around $\eta \approx 0.5$ for square shear wall; $\eta \approx 1.1$ for tall shear wall) as η increases from zero; but at $\theta_\beta = 30°$, regardless of the larger response at the second resonance near $\eta = 0.375$, $|\phi_0|$ is smaller beyond $\eta \approx 0.8$ away from resonant frequencies.

5. Summary

This paper presents results based on an approximate analytic procedure for solving the 2-dimensional, soil-structure-interaction problem excited by an incident plane SV wave. The approximation is based on relaxing the zero-stress boundary conditions on the half-space surface. It is shown that under such conditions, the wave function expansion becomes simple, and only half of the series representation for the scattered waves is required. Also, the closed-form solution depends only on finite-dimensional matrices and is easy to compute.

For cases of semi-circular foundation and shallow foundation when the incidence is below critical, numerical results on foundation displacements and shear wall responses agree well with those of [3]. For cases of shallow foundation when incident angles are beyond critical, numerical results are presented here for the first time. The agreement between the cases presented in this paper and those in [3] suggest that the free-surface boundary conditions are indeed not as essential as other conditions that govern the solution (the continuity of displacements along the contact surface between the half-space and foundation, and the dynamic equilibrium of the foundation). This result also supports the results of [7], which suggests that the solution to the model obtained from relaxed surface conditions may be similar to the solution in which a cylindrical approximation of the ground surface is made.

References

[1] Enrique Luco J. Dynamic interaction of a shear wall with the soil. J. Eng. Mech. Div. 1969;95:333–46.

[2] Trifunac MD. Interaction of a shear wall with the soil for incident plane SH waves. Bull. Seismol. Soc. Am. 1972;62(1):63–83.

[3] Todorovska MI. Trifunac MD. Analytical Model for in Plane Building-Foundation-Soil Interaction: Incident P-, SV-, and Raleigh Waves, Report No. 90-01, Dept. of Civil Engrg, Univ. of Southern California, pp. 122 (1990).

[4] Todorovska MI, Trifunac MD. In-plane foundation-soil interaction for embedded circular foundations. Soil Dyn. Earthq. Eng. 1993;12:283–97.

[5] Todorovska Maria I, Trifunac MD. Effects of the wave passage and the embedment depth for in-plane building-soil interaction. Soil Dyn. Earthq. Eng. 1993;12:343–55.

[6] Todorovska MI. Effects of the depth of the embedment on the system response during building-soil interaction. Soil Dyn. Earthq. Eng. 1992;11:111–23.

[7] Todorovska Maria I, Rjoub Yousef Al. Plain strain soil-structure interaction model for a building supported by a circular foundation embedded in a poroelastic half-space. Soil Dyn. Earthq. Eng. 2006;26:694–707.

[8] Lin Chi Hsin, Lee Vincent W, Todorovska Maria I, Trifunac Mihailo D. Zero-stress, cylindrical wave functions around a circular underground tunnel in a flat, elastic half-space: incident P waves. Soil Dyn. Earthq. Eng. 2010;30(10):879–94.

[9] Zhang Chao, Liu Qijian, Deng Peng. Surface motion of a half-space with a semi-cylindrical canyon under P, SV, and Rayleigh waves. Bull. Seismol. Am. 2017;107(2):1–13.

[10] Gičev Vlado, Trifunac Mihailo D, Orbović Nebojša. Translation, torsion, and wave excitation of a building during soil-structure interaction excited by an earthquake SH pulse. Soil Dyn. Earthq. Eng. 2015;77:391–401.

[11] Gičev Vlado, Trifunac Mihailo D, Orbović Nebojša. Two-dimensional translation, rocking, and waves in a building during soil-structure interaction excited by earthquake P-wave pulse. Soil Dyn. Earthq. Eng. 2016;90:454–66.

[12] Gičev Vlado, Trifunac Mihailo D, Orbović Nebojša. Two-dimensional translation, rocking, and waves in a building during soil-structure interaction excited by a plane earthquake SV-wave pulse. Soil Dyn. Earthq. Eng. 2016;88:76–91.